Biochimica et Biophysica Acta, 1103 (1992) 281–295

BBAMEM 75480

Immunological relatedness of the sarcoplasmic reticulum Ca^{2+}-ATPase and the Na^+,K^+-ATPase

Elek Molnar *, Sandor Varga **, Istvan Jona **, Norbert W. Seidler and Anthony Martonosi

Department of Biochemistry and Molecular Biology, State University of New York, Health Science Center at Syracuse, Syracuse, NY (USA)

(Received 17 July 1991)

Key words: ATPase, Ca^{2+}-; ATPase, Na^+/K^+-; ATPase, H^+/K^+-; Sarcoplasmic reticulum; Transverse tubular membrane; Monoclonal antibody; Anti-peptide antibody

The effect of anti-ATPase antibodies with epitopes near Asp-351 (PR-8), Lys-515 (PR-11) and the ATP binding domain (D12) of the Ca^{2+}-ATPase of sarcoplasmic reticulum (EC 3.6.1.38) was analyzed. The PR-8 and D12 antibodies reacted freely with the Ca^{2+}-ATPase in the native membrane, indicating that their epitopes are exposed on the cytoplasmic surface. Both PR-8 and D12 interfered with the crystallization of the Ca^{2+}-ATPase, suggesting that their binding sites are at interfaces between ATPase molecules. PR-11 had no effect on ATPase–ATPase interactions or on the ATPase activity of sarcoplasmic reticulum. The epitope of PR-11 is suggested to be the VIDRC sequence at residues 520–525, while that of D12 at residues 670–720 of the Ca^{2+}-ATPase. The use of predictive algorithms of antigenicity for identification of potential antigenic determinants in the Ca^{2+}-ATPase is analyzed.

Introduction

A wide selection of monoclonal and polyclonal Ca^{2+}-ATPase antibodies have been produced in recent years in several laboratories [1–21].

Studies with these antibodies defined the localization of Ca^{2+}-ATPase in the sarcoplasmic reticulum of whole muscle at various stages of development [1–4,7,8,13] and established a pattern of crossreactivity with various Ca^{2+}-ATPase isoenzymes [1–8,12,13,15, 19,21]. With the arrival of new information on the primary sequence [16,22–26] and three-dimensional structure of the Ca^{2+}-ATPase [27–36] it became possible to locate the epitopes for the various antibodies [9,10,11,14,16–18,20] and to relate their positions to functionally relevant sites in the three-dimensional structure of the Ca^{2+}-ATPase identified by covalent labeling with substrates, substrate analogues and fluorescent probes [9,11,14,19,37–40].

Although only few of the antibodies produced significant inhibition of ATPase activity and Ca^{2+} transport [5,9,11,14,19], several of them affected the interaction between ATPase molecules and interfered with the crystallization of Ca^{2+}-ATPase induced by vanadate [19].

Most of the antibodies are directed against the large cytoplasmic domains of the Ca^{2+}-ATPase [1,9–11,16,17,19] that contain the N- and C-terminal regions of the molecule [10] together with the phosphorylation and ATP binding sites [22,23,41]. Two antibodies were found to bind to 870–890 loop that is assumed to be located on the luminal surface of the sarcoplasmic reticulum [16,17].

The purpose of this report is to describe the properties of three antibodies that interact with the phospho-

* Permanent address: Institute of Biochemistry, Albert Szent-Gyorgyi University Medical School, H-6701 Szeged, Hungary.
** Permanent address: Central Research Laboratory, University Medical School, H-4012 Debrecen, Hungary.

Abbreviations: FITC, fluorescein 5'-isothiocyanate; CPA, cyclopiazonic acid; mAb, monoclonal antibody; SDS, sodium dodecyisulfate; SR, sarcoplasmic reticulum; Ca^{2+}-ATPase, the $Mg^{2+} + Ca^{2+}$-activated ATPase of sarcoplasmic reticulum (EC 3.6.1.38).

Correspondence: A. Martonosi, Department of Biochemistry and Molecular Biology, State University of New York, Health Science Center at Syracuse, Syracuse, NY 13210, USA.

rylation (PR-8), FITC binding (PR-11) and nucleotide binding regions (D12) of the Ca^{2+}-ATPase, respectively.

Experimental procedures

Materials

Antibody D12 was obtained from Dr. Angela F. Dulhunty, Dept. of Physiology and Experimental Pathology, John Curtin School of Medical Research, Australian National University, Canberra, A.C.T. 2601, Australia. Antibodies M10-P6-B7, M8-P1-A3 and M12-P4-E8 were provided by Dr William J. Ball, Dept. of Pharmacology and Cell Biophysics, University of Cincinnati College of Medicine, Cincinnati, OH 45267, USA. Antibodies PR-8 and PR-11 were supplied by Dr. Paul M. Rowe, Laboratory of Neurochemistry, National Institute of Neurological and Communicative Disorders and Stroke, National Institutes of Health, Bethesda, MD 20892, USA.

Methods

Preparation of sarcoplasmic reticulum

Sarcoplasmic reticulum vesicles were isolated from predominantly white skeletal muscles of New Zealand rabbits as described by Nakamura et al. [42], and the preparations were stored before use frozen at −70°C in 0.3 M sucrose, 10 mM Tris-maleate (pH 7.0) at a protein concentration of 30–40 mg/ml.

Preparation of cardiac microsomes

The preparation of cardiac microsomes was performed as described by Jones et al. [43]. The vesicles (10–12 mg protein/ml) were suspended in 0.25 M sucrose, 30 mM histidine (pH 7.4), frozen in liquid nitrogen, and stored at −70°C.

Preparation of transverse tubular membrane fraction

Transverse tubular membranes were isolated by discontinuous sucrose density centrifugation of skeletal muscle microsomes. Contaminating sarcoplasmic reticulum vesicles were loaded with Ca^{2+} in the presence of oxalate prior to centrifugation, allowing their separation from the light fraction enriched in transverse tubules as described by Rosemblatt et al. [44].

Labeling of Ca^{2+}-ATPase with fluorescein 5'-isothiocyanate (FITC)

The sarcoplasmic reticulum vesicles (2 mg protein/ml) were incubated at 25°C in 0.3 M sucrose, 50 mM Tris-HCl (pH 8.0), 5 mM $MgCl_2$ and 0.1 mM EGTA with 10 μM fluorescein 5'-isothiocyanate (5 nmol FITC/mg SR protein) for 30 min in the dark. The FITC stock solution (3 mM) was dissolved in ethanol. After labeling the samples were diluted 10-fold with 20 mM K-Mops (pH 7) centrifuged at 49000 × *g* at 2°C for 40 min to remove the unreacted dye and the sedimented vesicles were resuspended in 0.1 M KCl, 10 mM imidazole (pH 7.4) and 5 mM $MgCl_2$ [45].

Preparation of vanadate solutions

Stock solutions of monovanadate (50 mM) were prepared by boiling freshly made aqueous solutions of Na_3VO_4 at pH 10.0 for 15 min [38, 46]. Decavanadate solutions were prepared by adjusting the pH of a monovanadate stock solution to 4.0 and keeping the solution at 4°C overnight or longer [38,46]. The final pH was adjusted to 7 just before the experiment was started.

Partial tryptic proteolysis of sarcoplasmic reticulum

Tryptic digestion of sarcoplasmic reticulum proteins was carried out essentially as described by Dux and Martonosi [47]. Sarcoplasmic reticulum vesicles containing 2 mg protein per ml were digested with trypsin (0.05 mg/ml) in a medium of 0.1 M KCl, 10 mM imidazole (pH 7.4), supplemented either with EGTA and monovanadate or with Ca^{2+}, as described in the figure legends. The digestion was started after 5 min preincubation at 25°C by the addition of trypsin and aliquots were taken after 0, 0.25, 1, 5, 15, 30, 60 and 360 min. The proteolysis was stopped by the addition of 0.2 mg/ml soybean trypsin inhibitor.

SDS-polyacrylamide gradient gel electrophoresis

For SDS-polyacrylamide gradient gel electrophoresis the samples were dissolved in a solution of 5% sodium dodecyl sulfate, 10 mM Tris-HCl (pH 8.0), 1% β-mercaptoethanol, 10% glycerol, 0.05% Bromophenol blue. After incubation for 5 min at 100°C, aliquots containing 30–100 μg protein were applied for electrophoresis on 6–18% gradient gels according to Laemmli [48]. The fluorescent protein bands of FITC labeled SR were visualized in UV light from a MR-4 UV lamp from Gates, G.W. and Co., Franklin Square, Long Island, NY, USA. Permanent records were obtained by photographing the fluorescence emission on Kodak Plus-X pan film (ASA 125) through a Promaster Spectrum 7 yellow filter to absorb the reflected UV light. Exposure times were 0.5 to 2 min at f 8. The gels were stained either with Coomassie blue or with Stains-All. Before Stains-All staining SDS was removed from gels as described by Schibeci and Martonosi [49]; then 0.00125% Stains-All dissolved in 5% formamide, 25% 2-propanol, 15 mM Tris-HCl (pH 8.5) was applied in the dark for 12–18 h, followed by destaining with 10% 2-propanol for 18–36 h in the dark at room temperature. The electrophoretic transfer of proteins from SDS-polyacrylamide gels to nitro-

cellulose sheets and the procedures for immunostaining were described earlier [19].

Dot-blot analysis of antibody-antigen reaction specificity

To test cross reactivity of different antibodies, 2 μl of antigen solution containing 0.1–10 μg protein were spotted on nitrocellulose membrane. The binding of different antibodies (1:100–500 dilution) was tested with horseradish peroxidase conjugated anti-mouse and anti-rabbit IgG diluted to 1:1000. The bound conjugated IgG was visualized by the colored product of 4-chloro-1-naphthol as described by Molnar et al. [19].

Enzyme-linked immunoadsorbent assay (ELISA)

Sarcoplasmic reticulum proteins (0.03, 0.1, 0.3 and 1 μg) were immobilized on polyvinyl chloride microtiter wells (Bio-Rad, Inc., Richmond, CA 94804, USA) by incubation at 4°C overnight in 13 mM sodium carbonate, 35 mM sodium bicarbonate, pH 9.6. Blocking of non-specific protein binding was done by incubation with 1% bovine serum albumin in phosphate-buffered saline (PBS) solution containing 1.5 mM KH_2PO_4, 8.1 mM Na_2HPO_4, 0.137 M NaCl and 2.7 mM KCl (pH 7.2) for 1 h at room temperature. The reaction with different antibody containing media was performed for 1 h at 23°C. Plates were washed with PBS between each step. The plates were exposed to anti-mouse or rabbit IgG conjugated with horseradish peroxidase for 1 h. After washing the reaction was initiated with the addition of *o*-phenylenediamine according to Molnar et al. [19]. The developed color was read at 405 nm on a Titertek Multiskan microtitration plate photometer produced by Flow Laboratories, Inc., McLean, VA 22102, USA.

Crystallization of Ca^{2+}-ATPase and electron microscopy

The crystallization medium consisted of 0.1 M KCl, 10 mM imidazole (pH 7.4), 5 mM $MgCl_2$, 0.5 mM EGTA and 5 mM decavanadate. Sarcoplasmic reticulum protein concentration was 1 mg/ml. The formation of two-dimensional Ca^{2+}-ATPase crystals at 2°C can be seen within a few hours and becomes extensive after 24 h [50].

Antibody preparations were added either before or after crystallization of Ca^{2+}-ATPase. When added before crystallization the antibodies were preincubated with the sarcoplasmic reticulum vesicles at 2°C in 1:10 dilution for 1 h in 0.1 M KCl, 10 mM imidazole (pH 7.4) and 5 mM $MgCl_2$; after preincubation EGTA and vanadate were added to initiate crystallization. The crystallization was allowed to proceed for 48 h at 2°C, and samples were processed for electron microscopy.

Alternatively, Ca^{2+}-ATPase crystals were first induced by overnight incubation at 2°C in the vanadate-containing crystallization medium prior to adding antibodies at 1:10 final dilution. Aliquots were removed for electron microscopy after 1–2 h incubation at 2°C. For electron microscopy a small volume of the incubation mixture was deposited on a carbon coated parlodion film and negatively stained with 1% uranyl acetate, pH 4.3 at 2°C. The samples were viewed in a Siemens Elmiskop I microscope at 60 kV.

Computer analysis of amino acid sequences for antigenic determinants

Plots of the predicted secondary structures [51], antigenicities [52], chain flexibility [53], surface probability [54,55] and hydrophilicity [56] were made using a program kindly provided by Dr. R.S. Carmenes [57]. The analysis was based on the amino acid sequences of the slow and fast isoenzymes of the Ca^{2+}-ATPase [23]. Calculations were carried out at window sizes varied between 6 and 15; window 13 was used for the documentation included in this report.

Preparation of antibodies

The monoclonal antibody D12 was prepared as described by Dulhunty et al. [4] and was kindly provided to us by Dr. Angela F. Dulhunty. Antibodies M10-P6-B7, M8-P1-A3 and M12-P4-E8 were prepared according to Ball et al. [58], Ball and Lane [59] and Ball and Friedman [60]; they were provided to us by Dr. W.J. Ball. Antibodies PR-8 and PR-11 were prepared according to Rowe et al. [61] and were provided to us by Dr. P.M. Rowe.

Results

The interaction of the PR-8 antibody with the Ca^{2+}-ATPase

The polyclonal antibody PR-8 was produced in rabbits against a synthetic peptide (Table I) that contained the sequence of the *Torpedo* electric organ Na^+,K^+-ATPase in the region of the phosphate acceptor aspartyl residue [61]. The target peptide is homologous to the 345–357 sequence of the Ca^{2+}-ATPase of sarcoplasmic reticulum, that contains the phosphate acceptor aspartyl at position 351 (Table I).

The PR-8 antibody readily reacted with the sarcoplasmic reticulum Ca^{2+}-ATPase and with the dog kidney Na^+,K^+-ATPase, but there was only weak reaction with the H^+,K^+-ATPase of gastric mucosa (Fig. 1). In addition to the 100 kDa band of the Ca^{2+}-ATPase, there was also weak reaction in bands of $\simeq$ 60 kDa and $\simeq$ 40 kDa in the sarcoplasmic reticulum; these could represent either degradation products of the Ca^{2+}-ATPase or side reactions with other proteins.

Trypsin cleaves the Ca^{2+}-ATPase at the T_1 cleavage site (Arg-505) into two major fragments of 57 kDa (A) and 52 kDa (B) (Fig. 2). The A fragment is further cleaved at the T_2 cleavage site (Arg-198) into an A_1 subfragment (34 kDa) that contains the phosphate ac-

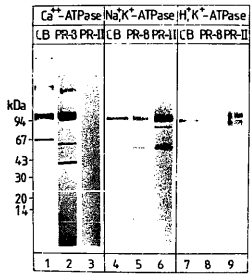

Fig. 1. The cross-reactivity of PR-8 and PR-11 antibodies with different ion transport ATPases. Rabbit fast skeletal muscle sarcoplasmic reticulum Ca^{2+}-ATPase (lanes 1–3), canine kidney medulla Na^+,K^+-ATPase (lanes 4–6), and H^+,K^+-ATPase from gastric mucosa (lanes 7–9) were separated by SDS-polyacrylamide electrophoresis on 6–18% gradient gels. The gels were stained with Coomassie blue (lanes 1, 4 and 7) or transferred to nitrocellulose sheets and incubated with 1:200 dilution of the PR-8 or PR-11 anti-peptide polyclonal rabbit antibodies. The bound antibodies were detected by reaction with horseradish peroxidase-conjugated anti-mouse IgG antibody as described under Methods.

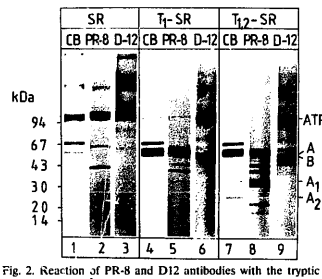

Fig. 2. Reaction of PR-8 and D12 antibodies with the tryptic fragments of the Ca^{2+}-ATPase. Sarcoplasmic reticulum proteins were partially digested with trypsin (25 μg trypsin/mg sarcoplasmic reticulum protein, 15 min at 25°C) in a medium of 0.1 M KCl, 10 mM imidazole-HCl (pH 7.4), 5 mM $MgCl_2$, supplemented either with 0.5 mM EGTA and 1 mM monovanadate for T1 cleavage yielding the A and B fragments, or with 0.1 mM $CaCl_2$ for T1 and T2 cleavage yielding A, A_1, A_2 and B fragments. The products of proteolysis were separated by SDS-polyacrylamide gel electrophoresis on 6–18% gradient gels and either stained with Coomassie blue or transferred to nitrocellulose sheets and incubated with 1:1000 (D12) or 1:200 (PR-8) dilutions of the antibodies, as described under Methods. Each sample contained the equivalent of 50 μg of sarcoplasmic reticulum protein. The bound antibodies were detected by reaction with horseradish peroxidase-conjugated anti-host IgG antibody. Lanes 1–3, native sarcoplasmic reticulum. Lanes 4–6, sarcoplasmic reticulum after tryptic cleavage of the Ca^{2+}-ATPase at the T1 site. Lanes 7–9, sarcoplasmic reticulum after tryptic cleavage of the Ca^{2+}-ATPase at the T1 and T2 sites. Lanes 1, 4 and 7: Coomassie blue staining. Lanes 2, 5 and 8: immunostaining with PR-8 antibody. Lanes 3, 6 and 9: immunostaining with D12 antibody.

ceptor Asp-351 residue and an A_2 subfragment (23 kDa) that represents the N-terminal one-fifth of the molecule (Fig. 2). The cleavage at the T2 site is prevented by vanadate in a Ca^{2+}-free solution [62]. Consistent with the proposed location of its epitope in the

TABLE I

Comparison of the amino acid sequences of the phosphorylation sites and the FITC binding sites of Na^+,K^+-ATPase and Ca^{2+}-ATPase

The sequence of the synthetic peptide that was used to develop antiserum PR-8 in rabbit [61] corresponds to amino acid 370–382 in the *Torpedo* electric organ Na^+,K^+-ATPase and to amino acids 363–375 in the bovine kidney Na^+,K^+-ATPase. This sequence contains the phosphate acceptor aspartyl residue. The analogous highly conserved sequences of the H^+,K^+-ATPase of pig gastric mucose (residues 380–392) and of the Ca^{2+}-ATPase of rabbit skeletal muscle sacroplasmic reticulum (residues 345–357) are shown below. The monoclonal antibody M8-P1-A3 directed against the lamb kidney Na^+,K^+-ATPase binds to a synthetic peptide, whose sequence corresponds to residues 496–506 of the Na^+,K^+-ATPase [58–60]. A similar synthetic peptide containing residues 505–517 of the *Torpedo* electric organ Na^+,K^+-ATPase was used to develop antiserum PR-11 in rabbit [61]. The corresponding sequences in the pig gastric mucose H^+,K^+-ATPase are residues 513–528, and in the rabbit fast skeletal muscle sacroplasmic reticulum Ca^{2+}-ATPase residues 510–525. The identical amino acids in the Na^+,K^+-ATPase and Ca^{2+}-ATPase are underlined. Fluorescein 5'-isothiocyanate specifically labels Lys-515 in the Ca^{2+}-ATPase, Lys-518 in the H^+,K^+-ATPase and Lys-501 in the lamb Na^+,K^+-ATPase.

Antibody	Target peptide		Source
PR-8	370 T S T I C S D K T G T L T	382	Na^+,K^+-ATPase (*Torpedo*)
	380 T S V I C S D K T G T L T	392	H^+,K^+-ATPase (pig gastric)
	345 T S V I C S D K T G T L T	357	Ca^{2+}-ATPase (rabbit SR)
M8-P1-A3	496 H L L V M K G A P E R	506	Na^+,K^+-ATPase (lamb)
PR-11	505 V M K G A P E R I L D R C	517	Na^+,K^+-ATPase (*Torpedo*)
	513 H V L V M K G A P E R V L E R C	528	H^+,K^+-ATPase (pig gastric)
	510 N K M F V K G A P E G V I D R C	525	Ca^{2+}-ATPase (rabbit SR)

region of the phosphate acceptor Asp-351 residue, the PR-8 antibody reacted only with the A fragment after digestion in the presence of EGTA and vanadate (Fig. 2; T_1 SR) and with the A and A_1 fragments after digestion in the presence of Ca^{2+} (Fig. 2, T_1, T_2 SR).

Based on ELISA, PR-8 reacted with the Ca^{2+}-ATPase in native sarcoplasmic reticulum vesicles both in the E_1 state stabilized by Ca^{2+} and in the E_2V state stabilized by vanadate in a Ca^{2+}-free medium (Fig. 3A), indicating that its epitope is exposed on the cytoplasmic surface of the membrane.

The vanadate-induced crystallization of the Ca^{2+}-ATPase (Fig. 4A) was prevented by preincubation of the sarcoplasmic reticulum vesicles with the PR-8 antibody (Fig. 4B), but addition of the antibody after crystallization did not cause the disruption of preformed Ca^{2+}-ATPase crystals (Fig. 4C). These observations suggest that the phosphorylation site of the Ca^{2+}-ATPase is located in a region of the ATPase structure, where the bound antibody can interfere with the ATPase-ATPase interactions required for crystallization, but once the crystals are formed, it still remains bound to the Ca^{2+}-ATPase. Therefore the interference with crystallization may be due to partial blocking of the interaction site.

The binding of PR-8 to the Ca^{2+}-ATPase did not inhibit the Ca^{2+}-stimulated ATP hydrolysis and had no effect on the vanadate- and Ca^{2+}-induced changes of the fluorescence of FITC-labeled Ca^{2+}-ATPase (not shown). Therefore the PR-8 antibody does not interfere with the binding of ATP and vanadate at the active site. Reciprocally, in a medium of 0.1 M KCl, 10 mM imidazole, 5 mM $MgCl_2$ and 0.1 mM Ca^{2+}, AMP-PNP (1 mM) and AMP-PCP (1 mM) had no effect on the binding of PR-8 to the Ca^{2+}-ATPase (Table II).

The interaction of PR-11 antibody with the Ca^{2+}-ATPase

The polyclonal PR-11 antibody was produced in rabbits against a synthetic polypeptide (Table I) containing the 505–517 sequence of the *Torpedo* electric organ Na^+,K^+-ATPase [61]. This sequence shows close homology with the 510–525 region of the sarcoplasmic reticulum Ca^{2+}-ATPase (Table I), that is adjacent to the primary tryptic cleavage site at Arg-505–Ala-506. Labeling of the Ca^{2+}-ATPase with fluorescein 5'-isothiocyanate at Lys-515 inhibits the ATPase activity and ATP-dependent Ca^{2+} transport, suggesting that this region of the molecule may be near the ATP binding site [63–65].

The PR-11 antibody interacted readily with the Na^+,K^+-ATPase and with the H^+,K^+-ATPase, but was bound relatively weakly to the Ca^{2+}-ATPase of sarcoplasmic reticulum either in the denatured (Fig. 1) or in the native state (Fig. 3B). The apparent affinity of PR-11 for the Ca^{2+}-ATPase was similar in the Ca_2E_1 and in the E_2-V conformations (Fig. 3B).

The low affinity of PR-11 for the Ca^{2+}-ATPase, as compared with the Na^+,K^+-ATPase, is probably related to the differences in amino acid sequence between the two enzymes near the FITC binding site (Table I). The PR-11 antibody did not cause significant impairment of the vanadate-induced crystallization of Ca^{2+} ATPase (Fig. 4D and E), and had no effect, even at relatively high concentration, on the Ca^{2+}-stimu-

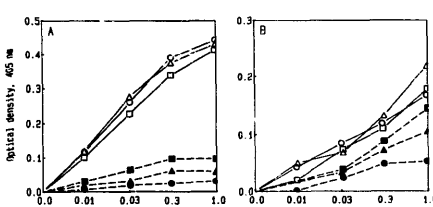

Fig. 3. Enzyme-linked immunoadsorbent (ELISA) assay of antibody binding to the Ca^{2+}-ATPase of sarcoplasmic reticulum in the E_1 and E_2V states. Sarcoplasmic reticulum vesicles (1 mg protein/ml) were preincubated with PR-8 (panel A) or PR-11 (panel B) antibodies at 1:10 dilution at 2°C for 1 h in a medium containing 0.1 M KCl, 10 mM imidazole, (pH 7.4), 5 mM $MgCl_2$ and either 0.5 mM $CaCl_2$ (E_1 state, ■---■) or with 0.5 mM EGTA and 5 mM Na_3VO_4 (E_2V state, ●---●, ▲---▲). Samples were taken before (●---● and after (▲---▲) the formation of vanadate-induced Ca^{2+}-ATPase crystals. In a parallel series of control experiments the antibodies were incubated under identical conditions in the absence of sarcoplasmic reticulum either in E_1 (□) or in E_2 (○, △) medium (solid lines). The unbound antibody was determined after centrifugation of the samples at 10000× *g* for 1 h by ELISA assay of the supernatant solutions at 1:10 dilution (total dilution of Ab 1:100), using sarcoplasmic reticulum vesicles absorbed to plastic in amounts of 0, 0.03, 0.1, 0.3 and 1 μg per well. The absorbance of the product of peroxidase reaction was determined at 405 nm, using a Titertek Multiskan microtitration plate photometer (Flow Laboratories, Inc.).

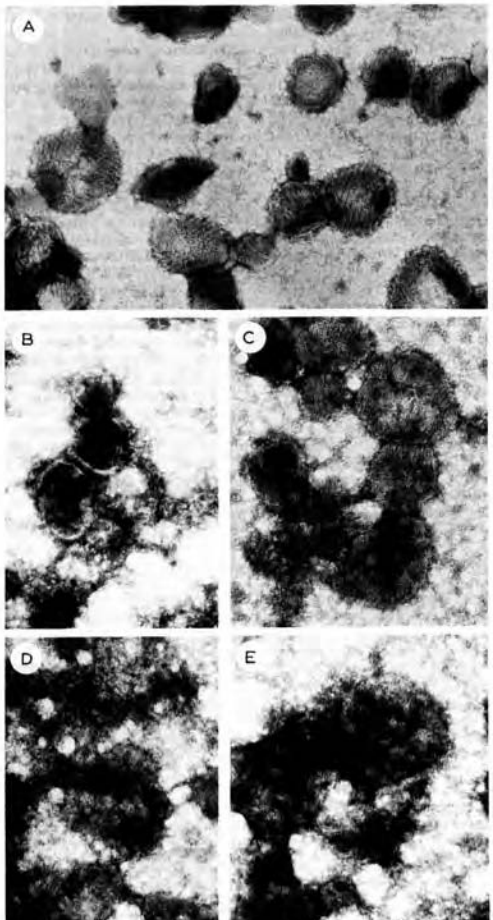
A
B
C
D
E

TABLE II

Effect of AMP-PNP and AMP-PCP on the binding of PR-8 and PR-11 antibodies to the Ca^{2+}-ATPase

Sacroplasmic reticulum vesicles (1 mg protein/ml) were incubated for 30 min at 2°C in a medium of 0.1 M KCl, 10 mM imidazole (pH 7.4), 5 mM $MgCl_2$, 0.1 mM $CaCl_2$ and 1 mM AMP-PNP or 1 mM AMP-PCP with PR-8 or PR-11 antibodies at 1:10 dilution. After centrifugation at 10000×*g* for 1 h the antibody content of the supernatant was assayed by ELISA at a final antibody dilution of 1:100 with 1 μg sacroplasmic reticulum protein fixed to the wells of the microtiter plate. Control antibody solutions were subjected to the same procedure except that sacroplasmic reticulum was omitted during preincubation. The absorbance of the product of peroxidase reaction was measured at 405 nm, as described under Methods. The difference in absorbance between the control samples and the samples obtained after preincbuation with the sacroplasmic reticulum was expressed as percent of the control absorbance.

Antibody	Antibody bound to SR, % of total		
	control	1 mM AMP-PNP	1 mM AMP-PCP
PR-8	47	45	47
PR-11	11	14	7

lated ATP hydrolysis. The weak binding of PR-11 was not affected by AMP-PNP (1 mM) or AMP-PCP (1 mM) either in the E_1Ca or in the E_2V state (Table II).

A monoclonal antibody M8-P1-A3 directed against the lamb Na^+,K^+-ATPase binds to an 11 residue peptide (Table I) that represents the 496–506 sequence of the lamb Na^+,K^+-ATPase [58–60]. This sequence partially overlaps with the sequence of the target peptide for PR-11, and with the homologous 510–520 region of sarcoplasmic reticulum Ca^{2+}-ATPase. Although M8-P1-A3 showed strong reaction in dot blots with the Na^+,K^+-ATPase of dog kidney medulla, it was entirely nonreactive with the native or denatured Ca^{2+}-ATPase in dot blots, Western blots or ELISA (not shown) under conditions where clear reactions were observed with PR-11. Since a portion of the target peptide sequence VMKGAPER is shared by the two antibodies (Table I), the antigenic determinant for the reaction of PR-11 with the Ca^{2+}-ATPase is probably the VIDRC sequence at 521–525 in the Ca^{2+}-ATPase and the homologous ILDRC sequence in the Na^+,K^+-ATPase.

The reaction of the monoclonal antibody D12 with the Ca^{2+}-ATPase

The monoclonal antibody D12 has similar affinity for the Ca^{2+}-ATPases isolated from rabbit fast-twitch and slow-twitch muscles [4]. Its epitope is exposed on the cytoplasmic surface of the membrane in native sarcoplasmic reticulum vesicles and after tryptic hydrolysis it was localized in the B tryptic fragment of the Ca^{2+}-ATPase (Fig. 2), representing the C-terminal half of the molecule. Binding of D12 to sarcoplasmic reticulum vesicles caused moderate inhibition of ATPase activity and Ca^{2+} transport at saturating concentration [19], together with some changes in the structure of Ca^{2+}-ATPase crystals induced by vanadate [19].

The binding site of D12 was further defined by following its interaction with a family of B fragments of decreasing size produced from FITC-labeled Ca^{2+}-ATPase by prolonged tryptic digestion in the presence of 0.5 mM EGTA (Fig. 5A,B), 5 mM $CaCl_2$ (Fig. 5C,D) or 0.5 mM EGTA and 5 mM vanadate (Fig. 5E,F). The B fragment is produced by hydrolysis of the Ca^{2+}-ATPase at the Arg-505–Ala-506 bond. Therefore the FITC bound at Lys-515 marks the N-terminal region of the B fragment, permitting its ready identification on polyacrylamide gels by monitoring the FITC fluorescence (Fig. 5A,C,E). With progressive digestion the molecular size of the fluorescent B fragment decreased from 52 kDa to ≈ 10 kDa due to the progressive removal of mass from its C-terminal end (Fig. 5). A family of distinct fluorescent subfragments (B_1 through B_7) formed, ranging in size from ≈ 30 kDa to ≈ 10 kDa (Fig. 5). After 6 h of digestion at 25°C in the presence of 0.5 mM EGTA (Fig. 5A) or 5 mM Ca^{2+} (Fig. 5C) essentially all the B fragment was hydrolyzed into the B7 subfragment. The rate of hydrolysis of the B fragment was slower in the media containing 0.5 mM EGTA and 5 mM vanadate (Fig. 5E), but despite this difference in the rate of hydrolysis, the size and distribution of the B_1-B_7 subfragments was similar under the three conditions (Fig. 5A,C,E).

The reaction of the D12 antibody with the products of proteolysis was analyzed after transfer to nitrocellulose sheets (Fig. 5B,D,F). In the undigested control samples the D12 antibody reacted with the intact Ca^{2+}-ATPase (≈ 109 kDa) and with an unidentified

Fig. 4. The effect of PR-8 and PR-11 antibodies on the stability of vanadate-induced two-dimensional Ca^{2+}-ATPase crystals. The crystallization of Ca^{2+}-ATPase was induced in sarcoplasmic reticulum vesicles (1 mg protein/ml) as described under Methods. Aliquots were negatively stained with 1% uranyl acetate and viewed in a Siemens Elmiskop I electron microscope at 60 kV. (A) Control sarcoplasmic reticulum after crystallization in the absence of antibodies. In B and D the sarcoplasmic reticulum vesicles were preincubated with 1:10 final dilution of PR-8 (B) or PR-11 (D) at 2°C for 1 h and then crystallization was initiated by the addition of vanadate-containing crystallization medium as described under Methods. In C and E the Ca^{2+}-ATPase crystals were first formed by overnight incubation at 2°C and the crystalline vesicles were incubated with PR-8 (C) or PR-11 (E) antibodies at 1:10 final dilution for 2 h at 2°C. Magnification: 112500×.

component of ≈ 80 kDa that may be a fragment of the Ca^{2+}-ATPase. During digestion at low trypsin concentration the antibody reaction moved first to the B fragment and then to the B_1 and B_2 subfragments, but there was no reaction associated with the smaller (B_3-B_7) subfragments even at high antibody concentration (Fig. 5B,D,F). Plots of the migration distances of the fluorescent B subfragments calibrated with molecular weight standards (not shown) establish that the minimum size of the fluorescent B subfragment that could

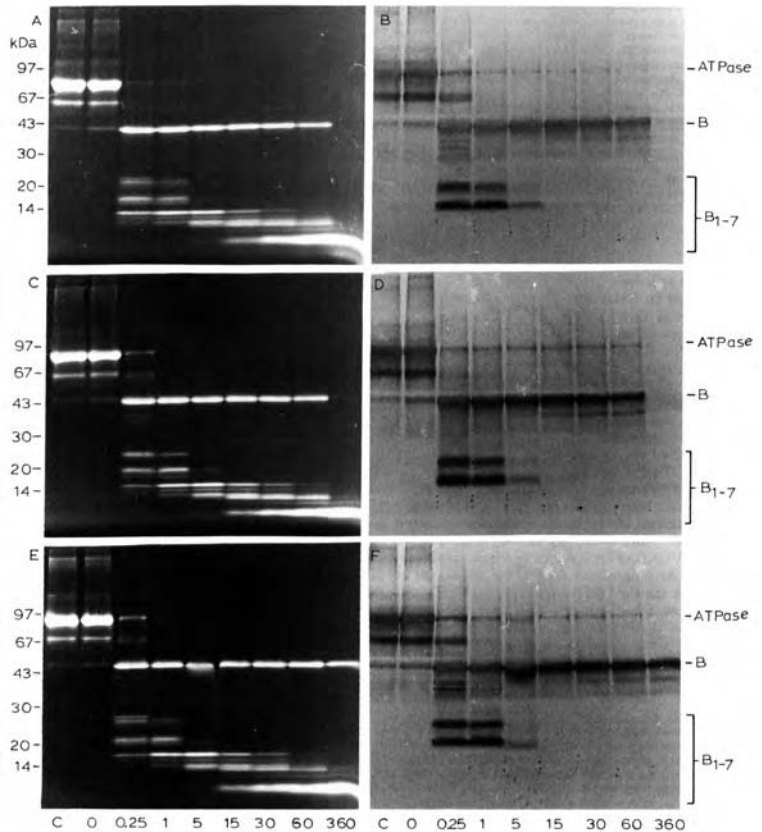

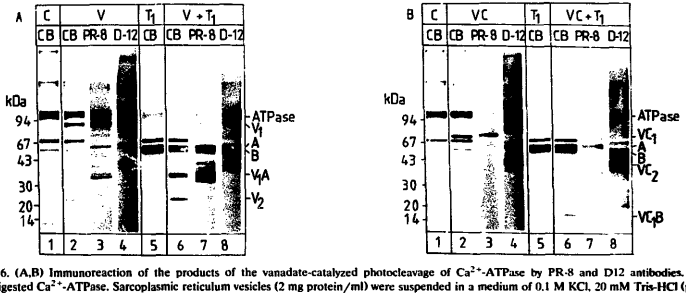

Fig. 6. (A,B) Immunoreaction of the products of the vanadate-catalyzed photocleavage of Ca^{2+}-ATPase by PR-8 and D12 antibodies. (i) Undigested Ca^{2+}-ATPase. Sarcoplasmic reticulum vesicles (2 mg protein/ml) were suspended in a medium of 0.1 M KCl, 20 mM Tris-HCl (pH 7.4), 5 mM $MgCl_2$, 1 mM monovanadate with either 1 mM EGTA (Fig. 6A, lanes 1–4) or 0.1 mM $CaCl_2$ (Fig. 6B, lanes 1–4). After illumination with ultraviolet light for 30 min, protein fragments were separated by SDS-polyacrylamide gel electrophoresis on 6–18% gradient gels, and either stained for protein with Coomassie blue or transferred to nitrocellulose sheets and reacted with PR-8 or D12 antibodies, as described under Methods. (ii) Ca^{2+}-ATPase after limited proteolysis. Proteolysis with trypsin (50 μg/ml) was performed in a medium of 0.1 M KCl, 10 mM imidazole HCl (pH 7.4), 5 mM $MgCl_2$, 0.5 mM EGTA and 1 mM monovanadate, at a microsomal protein concentration of 2 mg/ml at 25°C for 15 min; the reaction was stopped with 200 μg/ml soybean trypsin inhibitor. The samples were washed with a solution of 0.1 M KCl, 20 mM Tris-HCl (pH 7.4), 5 mM $MgCl_2$ and 50 μg/ml trypsin inhibitor by centrifugation at 105000 × g for 40 min at 2°C. The pellets were resuspended in the same solution and the samples were subjected to vanadate-catalyzed photocleavage with 1 mM EGTA (Fig. 6A, lanes 6–8) or with 0.1 mM $CaCl_2$ (Fig. 6B, lanes 6–8), as described above for the intact Ca^{2+}-ATPase. After transfer to nitrocellulose sheets the reaction with antibodies was performed as described under Methods. Each sample contained 50 μg of sarcoplasmic reticulum protein. Antibodies were diluted 1:1000 (D12) and 1:200 (PR-8) for reaction and the bound antibodies were detected using peroxidase-conjugated anti-host IgG antibody. Lane 1, sarcoplasmic reticulum (control; Coomassie blue staining). Lanes 2–4, sarcoplasmic reticulum after ultraviolet irradiation. Lane 2, Coomassie blue-stained fragments. Lane 3, immunostaining with PR-8 antibody. Lane 4, immunostaining with D12 antibody. Lane 5, sarcoplasmic reticulum after tryptic cleavage at the T1 site (Coomassie blue staining). Lanes 6–8, sarcoplasmic reticulum after tryptic cleavage of the Ca^{2+}-ATPase at the T1 site and ultraviolet irradiation. Lane 6, Coomassie blue staining of fragments. Lane 7, immunostaining with PR-8 antibody. Lane 8, immunostaining with D12 antibody.

react with the D12 antibody was of the order of 20 kDa. This locates the antigen for mAb D12 to a site between residues $\simeq 670$ and $\simeq 720$ in the primary structure of the Ca^{2+}-ATPase.

This localization was also tested by photochemical cleavage of Ca^{2+}-ATPase with vanadate as catalyst [38], followed by immunoreaction of the cleavage products (Fig. 6).

In the absence of calcium vanadate cleaves the Ca^{2+}-ATPase near the T_2 cleavage site (Arg 198), producing an N-terminal V_2 fragment of 22 kDa and a C-terminal V_1 fragment of 87 kDa [38]. In the presence of calcium the vanadate-catalyzed photocleavage occurs near residue 600 forming an N-terminal VC_1 fragment of 71 kDa and a C-terminal VC_2 fragment of 38 kDa [38]. The A and B tryptic fragments of Ca^{2+}-ATPase are cleaved by vanadate at the same locations as in the native ATPase. Photocleavage in the presence of Ca^{2+} cleaves the B tryptic fragment into a short VC_1B fragment (14 kDa) that contains the FITC binding site on Lys-515, and a C-terminal VC_2 fragment of the same size as that produced from the intact Ca^{2+}-ATPase. Photocleavage in the absence of Ca^{2+} cleaves the A tryptic fragment into the V_1 fragment (22 kDa)

Fig. 5. The reaction of the D12 monoclonal antibody with tryptic fragments of FITC-labeled sarcoplasmic reticulum Ca^{2+}-ATPase. FITC labeled sarcoplasmic reticulum (2 mg protein/ml) was partially digested with trypsin (25 μg trypsin/mg SR protein) at 25°C for 0, 0.25, 1, 5, 15, 30, 60 and 360 min as indicated on the abscissa. Samples labeled C were incubated without trypsin and trypsin inhibitor at 0°C and served as control. The basic digestion medium of 0.1 mM KCl and 10 mM imidazole (pH 7.4) was supplemented in panels A and B with 0.5 mM EGTA, in panels C and D with 5 mM $CaCl_2$ and in panels E and F with 0.5 mM EGTA, and 5 mM vanadate. The products of proteolysis were separated by SDS-polyacrylamide gel electrophoresis on 6–18% gradient gels. Since the T_1 cleavage site of the Ca^{2+}-ATPase is at Arg-505 and the FITC label is attached on Lys-515, the fluorescent peptides originate from the N-terminal region of the B tryptic fragment. With progressive digestion the molecular size of the fluorescent bands decreased from $\simeq 52$ kDa to $\simeq 10$ kDa due to removal of mass from the C-terminal end of the B fragment. Panels A, C and E show the fluorescence patterns of the gels using a long-wave mercury lamp for excitation as described under Methods. Panels B, D and F show the reaction of D12 mAb with the tryptic fragment of the Ca^{2+}-ATPase (30 μg protein/sample) after transfer to nitrocellulose sheets, as described under Methods. The positions of the Ca^{2+}-ATPase ($\simeq 110$ kDa), the B tryptic fragment ($\simeq 54$ kDa) and the B_{1-7} fragments (28–10 kDa) are indicated with corresponding symbols.

and a V_1A fragment of 35 kDa that is similar to the A_2 fragment obtained by tryptic cleavage at the T_2 site [38].

Based on this information the data shown in Fig. 6 can be interpreted as follows:

After photocleavage of native Ca^{2+}-ATPase with vanadate in the absence of Ca^{2+} (Fig. 6A, lanes 1–4), both the D12 and the PR-8 antibodies reacted with the large V_1 fragment. Following T_1 + V cleavage (Fig. 6A, lanes 5–8), the PR-8 reacted with the V_1A fragment that contains the phosphorylation site, while D12 reacted primarily with the B fragment and one of its large subfragments.

After photocleavage of the native Ca^{2+}-ATPase with vanadate in the presence of Ca^{2+} (Fig. 6B, lanes 5–8), the reaction of the D12 antibody was most intense in the VC_2 band containing the C terminal 1/3 of the molecule, while the PR-8 reaction was confined to the VC_1 region. The localization of D12 was unaffected by tryptic cleavage at the T_1 site, while the PR-8 reaction moved to the smaller A fragment (Fig. 6B, lanes 7 and 8).

Therefore the immunoreactions of D12 and PR-8 antibodies with the tryptic and vanadate cleavage fragments are consistent with the localization of their epitopes near the ATP binding (670–720) and phosphorylation domains (345–357), respectively.

The D12 antibody was specific for the skeletal muscle Ca^{2+}-ATPase and did not react significantly with any of the protein bands in cardiac sarcoplasmic reticulum, in dog kidney Na^+,K^+-ATPase and in pig H^+,K^+-ATPase preparations (not shown). The reaction observed in isolated T-tubule preparations was associated with a protein of the same size as the Ca^{2+}-ATPase of sarcoplasmic reticulum (not shown) and may be either due to contamination of T-tubules by sarcoplasmic reticulum vesicles or to a homologous T-tubule protein [66].

Other antibodies

Antibodies against the following short putative intramembrane segments of the Na^+,K^+-ATPase were provided by Dr. J. Kyte: LIFDNLK (492–498), ERKIVE (816–821), NSVFQQG (839–845) and KLVNER (836–841). None of these antibodies interacted with the Ca^{2+}-ATPase. Neither was any reaction observed with antibodies M10-P6-B7 and M12-P4-E8 directed against lamb kidney Na^+,K^+-ATPase [60].

Discussion

The properties of the anti-ATPase antibodies described in this report and in our earlier studies [19] are summarized in Table III. The following conclusions can be made. None of the 12 monoclonal antibodies directed against the fast-twitch skeletal muscle isoenzyme reacted with the cardiac Ca^{2+}-ATPase; reciprocally, the two mAb-s directed against the cardiac isoenzyme did not react with the rabbit skeletal isoform. Considering the extensive homology between the two proteins this would imply that the monoclonal antibodies are directed against a few highly antigenic regions that are different in the fast-twitch skeletal and the cardiac isoforms of the Ca^{2+}-ATPase. As expected, there was more extensive cross reaction by polyclonal antibodies between the two isoforms.

The PR-8 antibody [61] directed against the phosphate acceptor aspartyl group of the Na^+,K^+-ATPase had high affinity for the Ca^{2+}-ATPase, consistent with near identity of this region of the active site in the two enzymes. By contrast, the PR-11 antibody [61] directed against the conserved 503–517 sequence of the *Torpedo* Na^+,K^+-ATPase reacted only weakly with the Ca^{2+}-ATPase, while the M8-P1-A3 antibody [58–60] directed against a portion of the same sequence of the lamb Na^+,K^+-ATPase did not react at all with the Ca^{2+}-ATPase. We propose that the epitope for PR-11 contains the ILDRC sequence that is not represented in the target antigen for M8-P1-A3 (Table I), but it is present in slightly modified form (VIDRC) in the Ca^{2+}-ATPase (Table I). If this explanation is valid, the different affinity of PR-11 for the Na^+,K^+-ATPase and for the Ca^{2+}-ATPase can be attributed to the relatively small difference between the ILDRC and VIDRC sequences.

The general location of the antigenic sites within the various domains of the Ca^{2+}-ATPase was established for most of the anti-ATPase antibodies produced so far (Table III) by partial proteolysis with proteolytic enzymes and by vanadate-catalyzed photocleavage [1,4,14,16–20], but only a few monoclonal antibodies have their epitopes precisely defined [16–20].

To aid the identification of antigenic sites for the anti-ATPase antibodies we applied predictive algorithms of secondary structure [51], antigenicity [52], chain flexibility [53,67,68], surface probability [54,55] and hydrophilicity [56] to the primary structures of the slow- and fast-twitch isoenzymes of the Ca^{2+}-ATPase from skeletal muscle sarcoplasmic reticulum [23], using the program of Carmenes et al. [57]. The resulting plots are shown in Fig. 7A-D. As the various algorithms are based on different selection criteria, it is hoped that by analyzing the coincidence between them the reliability of prediction may be enhanced.

The *antigenicity plots* (Fig. 7B) are based on the percentages of amino acids present in known antigenic regions of 20 selected proteins, relative to the percentages of the same amino acids in the average composition of the proteins [52]. This empirical approach is perhaps the most direct, but its general applicability is not fully established.

TABLE III

Summary of the properties of anti-ATPase antibodies

The monoclonal and polyclonal antibodies used in these studies are listed together with information about their specificity, host species and cross-reactivity. For other details, see text. SSR, rabbit skeletal muscle sacroplasmic reticulum; CSR, rabbit cardiac sacroplasmic reticulum; fCa^{2+}-ATPase, the fast isoenzyme of rabbit sacroplasmic reticulum Ca^{2+}-ATPase; Na$^+$,K$^+$-ATPase was prepared from lamb or dog kidney medulla as marked. The sources of the various antibodies and their methods of preparation are listed under Materials.

Antibody		Antigen		Host species	Prepa-ration	[Protein] (mg/ml)	Cross reactivity							
							fCa^{2+}-ATPase				CSR Ca^{2+}-ATPase		dog Na$^+$,K$^+$-ATPase	
cod	type	species	enzyme				ELISA	dot blot	immuno-blot	antigen locus	ELISA	dot blot	dot blot	antigen locus
A25	mono	rabbit	SSR	mouse	IgG(p)	1.0	+	+	+	A_1 (328–505)	–	–	–	
IIH11	mono	rabbit	fCa^{2+}-ATPase	mouse	IgG(a)	30.4	+	+	+	A_1	–	–		
7C6	mono	rabbit	fCa^{2+}-ATPase	mouse	IgG(p)	2.4	+	+	+	A_1	–	–	–	
8A6	mono	rabbit	fCa^{2+}-ATPase	mouse	IgG(p)	3.9	+	+	+	A_1	–	–	–	
11A4	mono	rabbit	fCa^{2+}-ATPase	mouse	IgG(p)	3.9	+	+	+	A_1	–	–	–	
A22	mono	rabbit	fCa^{2+}-ATPase	mouse	IgM(p)	4.0	+	+	+	B (506–738)	–	–		
A52	mono	rabbit	fCa^{2+}-ATPase	mouse	IgG(p)	2.0	+	+	+	B (659–668)	–	–		
VE12$_1$G	mono	rabbit	fCa^{2+}-ATPase	mouse	IgG(a)	30.1	+	+	+	B	–	– +		
V1E8	mono	rabbit	fCa^{2+}-ATPase	mouse	IgG(a)	19.5	+	+	+	B	–	–		
5D2	mono	rabbit	fCa^{2+}-ATPase	mouse	IgG(p)	1.3	+	+	+	B	–	–	–	
4B4	mono	rabbit	fCa^{2+}-ATPase	mouse	IgG(p)	5.9	+	+	+	B	–	–		
D12	mono	rabbit	fCa^{2+}-ATPase	mouse	IgG(p)	2.0	+	+	+	B (670–720)	–	–	–	
1D8	mono	dog	CSR Ca^{2+}-ATPase	mouse	IgG(a)	23.0	–	–	–		+	+		
5C3	mono	chicken	SSR Ca^{2+}-ATPase	mouse	IgG(p)	2.0	–	–	–		–	–		
E	poly	rabbit	fCa^{2+}-ATPase	sheep	IgG(p)	5.0	+	+	+	$A_2 + A_1 + B$	+	+		
N	poly	rabbit	fCa^{2+}-ATPase	rabbit	serum	72.0	+	+	+	$A_1 2 + A_1 + B$	+	+		
EM-1	poly	rat	fCa^{2+}-ATPase	rabbit	serum	46.0	+	+	+	$A_2 + B$	+	+	–	
EM-2	poly	rat	fCa^{2+}-ATPase	rabbit	serum	63.0	+	+	+	$A_2 + A_1 + B$	+	+	–	
EM-3	poly	rat	fCa^{2+}-ATPase	rabbit	serum	73.0	+	+	+	$A_1 + A_1 + B$	+	+	–	
M10-P6-B7	mono	lamb	Na$^+$,K$^+$-ATPase	mouse	IgG(a)	17.3	+	–	–				+	
M8-P1-A3	mono	lamb	Na$^+$,K$^+$-ATPase	mouse	IgG(p)	1.0	–	–	–				+	(496–506) (Lamb)
M12-P4-E8	mono	lamb	Na$^+$,K$^+$-ATPase	mouse	IgG(p)	1.5	–	–	–				+	
Pr-8	anti-peptide poly	370 TSTICSDKTGTLT 382		rabbit	serum	62.5	+	+	+	A_1 (345–357)			+	(370–382) (*Torpedo*)
PR-11	anti-peptide poly	505 VMKGAPERILDRC 517		rabbit	serum	70.2	+	+	–	B (513–525)			+	(505–517) (*Torpedo*)

The *chain flexibility plot* (Fig. 7C) is based on the normalized temperature factors of the C_α atoms in high resolution crystals of 31 proteins, each of which were at least 50% different in sequence from all others [53].

The *surface probability* plot (Fig. 7D) analyzes the proportions of amino acid residues that are buried in the protein interior (solvent accessible surface area less than 20 Å^2), exposed on the protein surface (accessible surface more than 60 Å^2) or located in an intermediate environment (accessible surface 20–60 Å^2); the analysis was based on the crystal structures of 28 proteins [54,55].

The *hydrophilicity plot* (Fig. 7E) utilizes the solubility characteristics of amino acids to predict their exposure to solvents in the protein structure [56].

While all these properties (chain flexibility, surface exposure, hydrophilicity) are related to antigenicity, the predictive value of the various methods differs considerably [53,67,68]. According to Westhof et al. [67], antigenicity is better correlated with the segmental flexibility of the peptide chain than with its hydro-

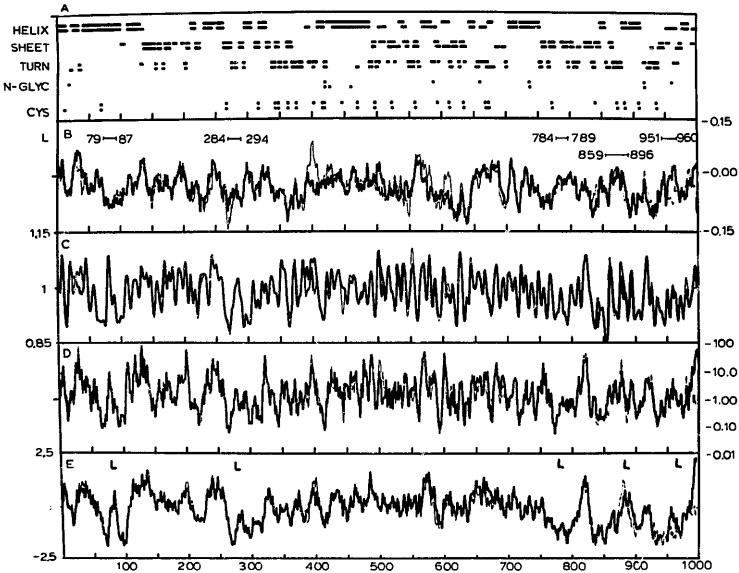

Fig. 7. Structural parameters of the Ca^{2+}-ATPase based on sequence. The structural analysis was performed using the program of Carmenes et al. [57] as described in Methods. The window size for antigenicity and hydrophilicity was 13. For the secondary structure predictions the Garnier's constants were −50 for helices and 0 for sheets. (Panel A) Predicted secondary structures, N-glycosylation sites and the locations of cysteine residues analyzed according to Garnier et al. [51]. The secondary structures of the slow isoenzyme are represented by the lines on top and that of the fast isoenzyme by the line underneath. (Panel B) Antigenicity [52]. The lines marked ——— indicate the probable segments exposed on the luminal side with flanking residue numbers. (Panel C) Chain flexibility [53]. (Panel D) Surface probability [54,55]. (Panel E) Hydrophilicity [56]. The letter L indicates the location of putative luminal segments with transmembrane helices on both sides. In panels B–E the predicted structural features of the fast isoenzyme (heavy line) and slow isoenzymes (fine line) of the Ca^{2+}-ATPase are superimposed to aid the identification of the differences between them.

philicity. Antipeptide antibodies directed against regions of high mobility react more strongly with the native protein than antibodies directed against well-ordered regions [68]. The high mobility of good antigenic determinants may facilitate the fit of the antibody into the antigenic site [67]. As loops, turns and the ends of polypeptide chains are highly flexible, they usually represent regions of high antigenicity [53].

As shown in Fig. 7, the slow and fast isoenzymes of Ca^{2+}-ATPase are represented by very similar plots of chain flexibility, surface probability and hydrophilicity (Fig. 7C,D,E), but there were significant differences between them in their predicted secondary structures and cysteine content (Fig. 7A), and in their antigenicity plots (Fig. 7B). The differences in the antigenicity plots are most pronounced in the sequences at 25–50, 260–275, 390–410, 425–500, 600–610 and 950–970; these differences may contribute to the isoenzyme specificity of antibody response.

The reliability of the prediction can be tested with antibodies whose epitopes are definitely established. Such are the PR-8 and PR-11 antibodies analyzed in this work, mAb A20 and A52 described by Clarke et al. [16], and the antipeptide antibodies described by Matthews et al. [17].

The epitope for PR-8 is in the 345–357 segment; this region is predicted to have high chain flexibility (Fig. 7C), moderate surface probability (Fig. 7D), and average hydrophilicity (Fig 7E). The binding site for PR-11 (510–525) has similar characteristics. Neither of these sites possesses particularly high antigenicity rating, based on the plots in Fig. 7B.

The epitope for mAb A52 at 657–672 [16] has relatively high predicted antigenicity by all five criteria, including the presence of turns. Antibodies D12 (this study), Y/3G6 and Y/2E9 [20] may also have epitopes in this region. There is no significant difference in antigenicity between the slow and fast isoenzymes of Ca^{2+}-ATPase in the 550–720 region of the molecule (Fig. 7B). This would be consistent with the observation of Dulhunty et al. [4] that D12 binds with similar affinity to the slow and fast isoenzymes of the Ca^{2+}-ATPase. Surprisingly, in our experiments D12 did not react significantly with the cardiac sarcoplasmic reticulum, either in ELISA or in dot blot assays. The absence of reaction with cardiac sarcoplasmic reticulum may be due in part to the much lower concentration of Ca^{2+}-ATPase in the cardiac membranes, but this point requires further investigation.

MAb A20 reacts with residues 870–890 in the proposed luminal segment of the Ca^{2+}-ATPase at 859–896 [16]. The same segment also reacts with a polyclonal antipeptide antibody directed against residues 877–888 [17]. This site is exposed to antibodies only after solubilization with detergents or permeabilization by EGTA. The site has high antigenicity based on all criteria including high flexibility, surface exposure and β turn potential (Fig. 7A–E).

The sites of reaction of antipeptide antibodies directed against the N terminus (residues 1–12) and the C terminus (residues 985–994) of the Ca^{2+}-ATPase [17] are also among the regions of highest predicted antigenicity.

Therefore the algorithms correctly predict the binding sites of antibodies with known epitopes as regions of above average antigenicity, although there is some variation between the different methods in the strength of prediction.

The region of high predicted antigenicity at 560–590 may serve as binding site for antibodies Y/1F4, Y/3G6, Y/2E9 and Y/3C8; the epitopes of these antibodies were localized by proteolysis to the 547–641 region of the Ca^{2+}-ATPase [14,20]. The monoclonal antibody 1/2H7 was found to bind to the Asp-Asp-Ser-Ser-Arg-Phe-Met-Glu-Tyr sequence (579–587) within this region [20]. The 560–590 region may also bind mAb A22, VE12G9, V1E8, 5D2 and 4B4 described in our earlier report [19].

Antibodies Y/3H5 and Y/1H12 with suggested binding sites in the 249–376 region [20] may have their epitopes either at residues 320–340 or at the segment of high predicted antigenicity and turn content at residues 390–410. This site is a strong candidate for binding mAb 7C6, one of the few antibodies that react with the A_1 region of the Ca^{2+}-ATPase in the native sarcoplasmic reticulum [19].

The monoclonal antibody A25 [16] with epitope in the 330–505 region presents a special case; its binding site is not available for reaction either in the native or in the $C_{12}E_8$-solubilized sarcoplasmic reticulum, but becomes exposed after denaturation in SDS. Based on this behavior, its antigenic site is not likely to possess high surface probability or hydrophilicity, but should retain good antigenicity. A site that would fit these criteria within the 330–505 region is the 410–420 segment characterized by low surface probability and hydrophilicity (Fig. 7D,E), but above average antigenicity (Fig. 7B). The same region may also bind IIH11, 8A6 and IIA4 [19], all of which have masked antigenic sites in the A_1 region of the native enzyme. Further work is needed to validate these predictions.

Acknowledgements

This study was supported by research grants from the National Institutes of Health (AR 26545), the National Science Foundation (88–23077 and Int. 86–17848) and by a grant-in-aid from the Muscular Dystrophy Association.

References

1 Zubrzycka-Gaarn, E., MacDonald, G., Phillips, L., Jorgensen, A.O. and MacLennan, D.H. (1984) J. Bioenerg. Biomembr. 16, 441–464.
2 Leberer, E. and Pette, D. (1986) Eur. J. Biochem. 156, 489–496.
3 Kaprielian, Z. and Fambrough, D.M. (1987) Dev. Biol. 124, 490–503.
4 Dulhunty, A.F., Banyard, M.R.C. and Medveczky, C.J. (1987) J. Membr. Biol. 99, 79–92.
5 Levitsky, D.O., Syrbu, S.I., Cherepakhin, V.V. and Rokhlin, O.V. (1987) Eur. J. Biochem. 164, 477–484.
6 Sarkadi, B., Enyedi, A., Penniston, J.T., Verma, A.K., Dux, L., Molnar, E. and Gardos, G. (1988) Biochim. Biophys. Acta 939, 40–46.
7 Jorgensen, A.O., Arnold, W., Pepper, D.R., Kalil, S.D., Mandel, F. and Campbell, K.P. (1988) Cell Motil. Cytoskel. 9, 164–174.
8 Krenacs, T., Molnar, E., Dobo, E. and Dux, L. (1989) Histochem. J. 21, 145–155.
9 Matthews, I., Colyer, J., Mata, A.M., Lee, A.G., Green, N.M. and East, J.M. (1989) Biochem. Soc. Trans. 17, 708–709.
10 Matthews, I., Colyer, J., Mata, A.M., Green, N.M., Sharma, R.P., Lee, A.G. and East, J.M. (1989) Biochem. Biophys. Res. Commun. 161, 683–688.
11 Mata, A.M., Lee, A.G. and East, J.M. (1989) FEBS Lett. 253, 273–275.
12 Wuytack, F., Kanmura, Y., Eggermont, J.A., Raeymaekers, L., Verbist, J., Hartweg, D., Gietzen, K. and Casteels, R. (1989) Biochem. J. 257, 117–123.
13 Karin, N.J., Kaprielian, Z. and Fambrough, D.M. (1989) Mol. Cell. Biol. 9, 1978–1986.
14 Colyer, J., Mata, A.M., Lee, A.G. and East, J.M. (1989) Biochem. J. 262, 439–447.
15 Wuytack, F., Eggermont, J.A., Raeymaekers, L., Plessers, L. and Casteels, R. (1989) Biochem. J. 264, 765–769.
16 Clarke, D.M., Loo, T.W. and MacLennan, D.H. (1990) J. Biol. Chem. 265, 17405–17408.
17 Matthews, I., Sharma, R.P., Lee, A.G. and East, J.M. (1990) J. Biol. Chem. 265, 18737–18740.
18 Mata, A.M., Michelangeli, F., Lee, A.G. and East, J.M. (1990) Biochem. Soc. Trans. 18, 603.
19 Molnar, E., Seidler, N.W., Jona, I. and Martonosi, A. (1990) Biochim. Biophys. Acta 1023, 147–167.
20 Tunwell, R.E.A., O'Connor, C.D.O., Mata, A.M., East, J.M. and Lee, A.G. (1991) Biochim. Biophys. Acta 1073, 585–592.
21 De Foor, P.H., Levitsky, D., Birjukova, T. and Fleischer, S. (1980) Arch. Biochem. Biophys. 200, 196–205.
22 MacLennan, D.H., Brandl, C.J., Korczak, B. and Green, N.M. (1985) Nature 316, 696–700.
23 Brandl, C.J., Korczak, B., Green, N.M. and MacLennan, D.H. (1986) Cell 44, 597–604.
24 Clarke, D.M., Loo, T.W., Inesi, G. and MacLennan, D.H. (1989) Nature 339, 476–478.
25 Clarke, D.M., Maruyama, K., Loo, T.W., Leberer, E., Inesi, G. and MacLennan, D.H. (1989) J. Biol. Chem. 264, 11246–11251.
26 Clarke, D.M., Loo, T.W. and MacLennan, D.H. (1990) J. Biol. Chem. 265, 6262–6267.
27 Taylor, K.A., Dux, L. and Martonosi, A. (1984) J. Mol. Biol. 174, 193–204.
28 Castellani, L., Hardwicke, P.M.D. and Vibert, P. (1985) J. Mol. Biol. 185, 579–594.
29 Taylor, K.A., Dux, L. and Martonosi, A. (1986) J. Mol. Biol. 187, 417–427.
30 Taylor, K.A., Ho, M.H. and Martonosi, A. (1986) Ann. N.Y. Acad. Sci. 483, 31–43.
31 Taylor, K.A., Mullner, N., Pikula, S., Dux, L., Peracchia, C., Varga, S. and Martonosi, A. (1988) J. Biol. Chem. 263, 5287–5294.
32 Stokes, D.L. and Green, N.M. (1990) Biophys. J. 57, 1–14.
33 Stokes, D.L. and Green, N.M. (1990) J. Mol. Biol. 213, 529–538.
34 Stokes, D.L. and Green, N.M. (1990) Biochem. Soc. Trans. 18, 841–843.
35 Blasie, J.K., Herbette, L. and Pachence, J. (1985) J. Membr. Biol. 86, 1–7.
36 Blasie, J.K., Pascolini, D., Asturias, F., Herbette, L.G., Pierce, D. and Scarpa, A. (1990) Biophys. J. 58, 687–693.
37 Squier, T.C., Bigelow, D.J., De Ancos, G.J. and Inesi, G. (1987) J. Biol. Chem. 262, 4748–4754.
38 Vegh, M., Molnar, E. and Martonosi, A. (1990) Biochim. Biophys. Acta 1023, 168–183.
39 Martonosi, A.N., Jona, I., Molnar, E., Seidler, N.W., Buchet, R. and Varga, S. (1990) FEBS Lett. 268, 365–370.
40 Jona, I., Matko, J. and Martonosi, A. (1990) Biochim. Biophys. Acta 1028, 183–199.
41 Green, N.M., Taylor, W.R. and MacLennan, D.H. (1988) in The Ion Pump: Structure, Function and Regulation (Stein, W., ed.), pp. 15–24, Alan R. Liss, New York.
42 Nakamura, H., Jilka, R.L., Boland, R. and Martonosi, A. (1976) J. Biol. Chem. 251, 5414–5423.
43 Jones, L.R. and Cala, S.E. (1981) J. Biol. Chem. 256, 11809–11818.
44 Rosenblatt, M., Hidalgo, C., Vergara, C. and Ikemoto, N. (1981) J. Biol. Chem. 256, 8140–8148.
45 Papp, S., Pikula, S. and Martonosi, A. (1987) Biophys. J. 51, 205–220.
46 Csermely, P., Varga, S. and Martonosi, A. (1985) Eur. J. Biochem. 150, 455–460.
47 Dux, L. and Martonosi, A. (1983) J. Biol. Chem. 258, 2599–2603.
48 Laemmli, U.K. (1970) Nature 227, 680–685.
49 Schibeci, A. and Martonosi, A. (1980) Anal. Biochem. 104, 335–342.
50 Dux, L. and Martonosi, A. (1983) J. Biol. Chem. 258, 11896–11902.
51 Garnier, J., Osguthorpe, D.J. and Robson, B. (1978) J. Mol. Biol. 120, 97–120.
52 Welling, G.W., Weiser, W.J., Van der Zee, R. and Welling-Wester, S. (1985) FEBS Lett. 188, 215–218.
53 Karplus, P.A. and Schulz, G.E. (1985) Naturwissenschaften 72, 212–213.
54 Janin, J., Wodak, S., Levitt, M. and Maigret, M. (1978) J. Mol. Biol. 125, 357–386.
55 Emini, E.A., Hughes, J.V., Perlow, D.S. and Boger, J. (1985) J. Virol. 55, 836–839.
56 Hopp, T.P. and Woods, K.R. (1981) Proc. Natl. Acad. Sci. USA 78, 3824–3828.
57 Carmenes, R.S., Freise, J.P., Molina, M.M. and Martin, S.M. (1989) Biochem. Biophys. Res. Commun. 159, 687–693.
58 Ball, W.J., Schwartz, A. and Lessard, J.L. (1982) Biochim. Biophys. Acta 719, 413–423.
59 Ball, W.J. and Lane, L.K. (1986) Biochim. Biophys. Acta 873, 79–87.
60 Ball, W.J. and Friedman, M.L. (1987) Biochem. Biophys. Res. Commun. 148, 246–253.
61 Rowe, P.M., Link, W.T., Hazra, A.K., Pearson, P.G. and Albers, R.W. (1988) in The Na^+,K^+ pump, Part A: Molecular Aspects (Skou, J.C., Norby, A.B., Maunsbach, A.B. and Esman, M. eds.), pp. 115–120, Alan R. Liss, New York.
62 Dux, L. and Martonosi, A. (1983) J. Biol. Chem. 258, 10111–10115.

63 Pick, U. and Bassilian, S. (1981) FEBS Lett. 123, 127–130.
64 Mitchinson, C., Wilderspin, A.F., Trinnaman, B.J. and Green, N.M. (1982) FEBS Lett. 146, 87–92.
65 Champeil, P., Riollet, S., Orlowski, S., Guillain, F., Seebregts, C.J. and McIntosh, D.B. (1988) J. Biol. Chem. 263, 12288–12294.
66 Kirley, T.L. (1988) J. Biol. Chem. 263, 12682–12689.
67 Westhof, E., Altschuk, D., Moras, D., Bloomer, A.C., Mondragon, A., Klug, A. and Van Regenmortel, H.H.V. (1984) Nature 311, 123–126.
68 Tainer, J.A., Getzoff, E.D., Alexander, H., Houghten, R.A., Olson, A.J. and Lerner, R.A. (1984) Nature 312, 127–134.